Construction and Building Materials 395 (2023) 132186

Contents lists available at ScienceDirect

Construction and Building Materials

journal homepage: www.elsevier.com/locate/conbuildmat

Improving the interface compatibility and mechanical performances of the cementitious composites by low-cost alkyl ketene dimer modified fibers

Helong Song, Tao Liu, Florent Gauvin *, H.J.H. Brouwers

Department of the Built Environment, Eindhoven University of Technology, P. O. Box 513, 5600 MB Eindhoven, The Netherlands

ARTICLE INFO

Keywords:
Hemp fiber
Fiber surface treatments
Interface compatibility
Fiber reinforced cement composites
Mechanical strength

ABSTRACT

Natural fibers-reinforced cement composites have recently attracted more interest due to the trend in the development of sustainable construction materials. However, the poor fiber–matrix interface compatibility, which is caused by the swelling-shrinking behavior of hydrophilic natural fiber, negatively affects the mechanical properties of the composites thereby hindering their practical application. In order to promote interfacial compatibility, a new fiber surface treatment is needed. A low-cost alkyl ketene dimer (AKD) is adopted in this work, aiming at replacing the relatively expensive silane agents. This study focuses on fiber surface treatment and the resulting effects on the interface compatibility and mechanical performances of the composites. The effect of the fiber modification was characterized by FTIR and water absorption test; The interfacial compatibility of the composites was evaluated by the compatibility index calculation and SEM observation; A series of strength properties of the composites were carried out considering the influence of interface compatibility on mechanical performance. Results show a clear improvement in both interface compatibility and mechanical properties of the composites when AKD-modified fibers are used as reinforcement. The compressive and flexural strength are effectively increased up to 53 MPa and 8 MPa, respectively. Moreover, the approach of the low-cost AKD modification could further be applied to any natural fibers in cementitious composites, allowing cost-effectiveness in practical applications.

1. Introduction

Fiber-reinforced cement composites have received a lot of attention in recent decades due to their good flexural performance, which can be needed in some special applications that require high toughness of the cement matrix [1]. For example, these composites have the potential to be applied in river levees [2], bridge decks [3,4], agricultural by-products like [5,6], columns and beams [3], cladding panels [6], and roof sheet and siding [7]. It is known that pure cementitious materials have low ultimate tensile strain, tensile strength, and impact strength, and can easily crack, although these kinds of materials have good compressive properties. Thus, adding fibers to the cement matrix is an effective measure to improve the above drawbacks [8].

Steel fiber [9], carbon fiber [10] and synthetic polymer fibers such as polypropylene (PP) [11], polyethylene (PE) [12], and polyvinyl alcohol (PVA) fiber [13] have been studied as reinforcement in cement composites for several decades. In recent years, considering their advantages in terms of sustainability and cost, natural fibers have also been investigated as potential reinforcement in the cementitious matrix. However, natural fiber-reinforced cement composites have been characterized to have low durability and poor cement compatibility [14] on account of the fiber's degradation [15,16] and mineralization [15,17] under the alkaline cementitious matrix, as well as the swelling-shrinking behavior caused by the moisture absorption characteristic [18,19]. In detail, for the degradation of fiber, lignin, hemicellulose, and part of the cellulose of natural fibers are hydrolyzed and degraded under the attack of OH^- produced from the cement hydration [20]. At the same time, fiber mineralization is caused by the deposition of portlandite and calcite on the natural fiber [21]. In addition, the swelling phenomenon before the shrinking of natural fiber is explained by the important number of hydroxyl groups that existed in the amorphous zone of the fiber [19]. The above problems have a negative influence on the strength performance (compressive strength, flexural strength, and toughness capacity) of the composites; hence the effect of modified fiber–matrix interface on the strength properties of composites has been focused on and studied these years.

Many researchers have used different chemicals to modify the fiber surface to reinforce geopolymer and cement matrices. For example,

* Corresponding author.
E-mail address: f.gauvin@tue.nl (F. Gauvin).

https://doi.org/10.1016/j.conbuildmat.2023.132186
Received 14 April 2023; Received in revised form 14 June 2023; Accepted 15 June 2023

Janne et al. [22] treated abaca fiber with 6 wt% NaOH solution to reinforce foamed geopolymer composites. The results showed that both the compressive strength and flexural strength of alkali-treated fiber composite were increased. Besides that, the appearance of treated fibers was rougher and more uniform by SEM observations, which could, in theory, facilitate the fiber–matrix interlocking. Tonoli et al. [23] investigated the pulp fibers modified with aliphatic isocyanate (AI) to reinforce a cement matrix. It was observed that the elasticity modulus of the treated composite was improved whereas the water absorption of these AI-treated fibers also decreased. Ban et al [24] studied the effect of bamboo fibers with glycerol and aluminate ester on the properties of bamboo fiber-reinforced cement mortars. The results showed that the glycerol modification can increase the flexural strength of the resulting composites and aluminate ester treatment allowed the composites to possess optimum properties like impermeability, chloride resistance, and carbonization. In addition, silane coupling agents are commonly used to improve the cross-link between the fiber and the matrix in composites. Bilba and Arsene [25] have reported that silane coating of fibers has the advantage of improving the fiber–matrix interface and reducing water absorption. Yet, such treatment does not show long-term performance as cellulose-O-Si-O-bonds are not stable against hydrolysis [26,27]. Especially under the alkaline condition of the cement hydration process, the chemical bond rupture between silanes and cellulose occurs readily as acids and bases are known to be powerful catalysts for the hydrolysis of siloxane bonds [28]. In addition to these technical difficulties, the cost of fiber modifying agents also has to be considered (commonly silane coupling agents, 20–50 €/kg) Therefore, it is urgent to look for a new and low-cost modifying agent to treat the fibers which can (1) bind chemically to cellulosic fibers to change the hygroscopic character of natural fibers; (2) be stable under alkaline conditions; (3) be economic.

Hydrophobic modification of natural fiber is a common treatment to resist liquid penetration in papermaking, which is called surface sizing. low-cost alkyl ketene dimer (AKD, 1–10 €/kg) is a main sizing agent resulting in enhanced water resistance [29]. Zhang et al [30] investigated the effect of bamboo flour with alkyl ketene dimer (AKD) on the polyethylene/bamboo flour composites. It was observed that AKD-modified wood-plastic composites had high water resistance, low swelling ratio, and excellent mechanical properties. Angin et al [31] analyzed the chemical and thermal properties of using AKD as a coupling agent for natural fiber and glass fiber-reinforced poly composites. The results indicated that the crystallinity of the hybrid composites was increased by 18% compared to neat composites. Missoum et al [32] used AKD to chemically modify nano-fibrillated cellulose (NFC) and found that AKD modification can increase the mechanical property of the resulting NFC. Though most researchers are focusing on utilizing AKD for improving the properties of natural fibers, to our knowledge none of them has reported AKD-modified fiber used in cementitious composites. Furthermore, given the alkaline resistance of the embedded fiber in fiber-reinforced cement composites and its relatively low cost, AKD seems to be a promising candidate.

In this study, hemp fiber is selected considering tons of waste hemp produced in Europe [33]. To begin with, fibers were pretreated (acetone and alkali treatment), then grafting modified with AKD, and finally mixed in a cementitious matrix to form composites. The main aim of this work is to explore the effect of hemp fiber's modification on the interfacial compatibility and mechanical performances of the composites. To be more specific, the interface microstructure, reaction productions of the cement matrix, and the strength properties of the composites are analyzed. The presented results provide fundamental insights into the greatly improved interface bonding performance and enhanced strength property.

Table 1
Physical properties of hemp fibers.

Diameter (mm)	Density (g/cm^3)	Average length (mm)	Aspect ratio	Water absorption (%)	Young's modulus (GPa)
0.25 ± 0.08	1.34	4.23	8–28	141	20.5

Table 2
Chemical compositions of hemp fibers (wt. %) [34].

Fiber type	Cellulose	Lignin	Hemicellulose	Pectin	Wax
Hemp fiber	70.2–74.4	3.7–5.7	17.9–22.4	0.9	0.8

2. Experimental

2.1. Materials

Hemp fiber products (designated"H") were supplied by HempFlax (The Netherlands). Before the experiments, hemp fibers were sieved, washed, and dried because many broken inner stems and fine fibers (<1 cm length) existed. In addition, the chemical compositions of hemp fibers are mainly cellulose, lignin, hemicellulose, waxes, and water-soluble substances. The detailed physical properties and chemical components of the hemp fiber are listed in Table 1 and Table 2, respectively.

The commercial alkyl ketene dimers emulsion was provided by Kemira (Finland). Commercial ordinary Portland cement (OPC) CEM I 52.5R (Specific surface area 1.34 m^2/g) was supplied by ENCI (The Netherlands). The oxide compositions, phase compositions, and particle size distribution of the OPC are shown in Table 3 and Fig. 1.

The standard sands with a granulometry of 0/2 were used according to EN 196–1. The particle size distribution of used sand was shown in Fig. 2.

2.2. Methods

2.2.1. Fiber treatments

To better modify hemp fiber, pre-treatments were employed on hemp fiber. Pre-treatment involves two steps: de-waxing, and alkali treatment [28]. Firstly, the wax was almost entirely taken out of the fibers (90% of 2–4 mm length, around 125 μm diameter) using ultra-pure acetone. The fibers were kept in jacketed Erlenmeyer flasks with boiling acetone for 45 min. Then, the fibers were immersed in 5 wt% sodium hydroxide solution for 30 mins and immediately washed with distilled water. To fully neutralize the effect of NaOH, a weak acetic acid solution was applied to reach the neutral pH. Subsequently, distilled water was utilized to rinse the fibers. After that, the fibers were dried at room temperature for 48 h and then in an oven at 70 ℃ for 8 h.

The fiber modification was carried out using a similar procedure proposed by H. Zhang et al. [35]. Hemp fibers (H) and hemp fibers after pretreatment (HP) were impregnated with a 2.4% AKD emulsion for 1.5 h, and then impregnated fibers were filtered by vacuum filtration equipment. Finally, these modified fibers (HPM) were dried in the oven at 90 ℃ for 6 h.

2.2.2. Preparation of fiber-reinforced composites

Hemp fiber-reinforced composites with 1% (by weight relative to cement weight) of short hemp fibers (0.2 ~ 0.8 cm) were prepared from the untreated and treated fibers. Firstly, this amount of fiber addition is determined based on the optimal addition of the literature [36,37]. Secondly, the selection of short fibers in this study is considered: one is a lot of short fibers are wasted, not applied in the textile industry like long hemp fibers [38]; the other is to take advantage of easily random

Table 3
Chemical composition of OPC (wt. %).

Compounds	MgO	Al_2O_3	SiO_2	K_2O	CaO	TiO_2	Fe_2O_3	SO_3	In_2O_3	Rest
CEM I	1.48	4.25	17.32	0.5	67.62	0.4	3.26	3.03	1.32	0.82

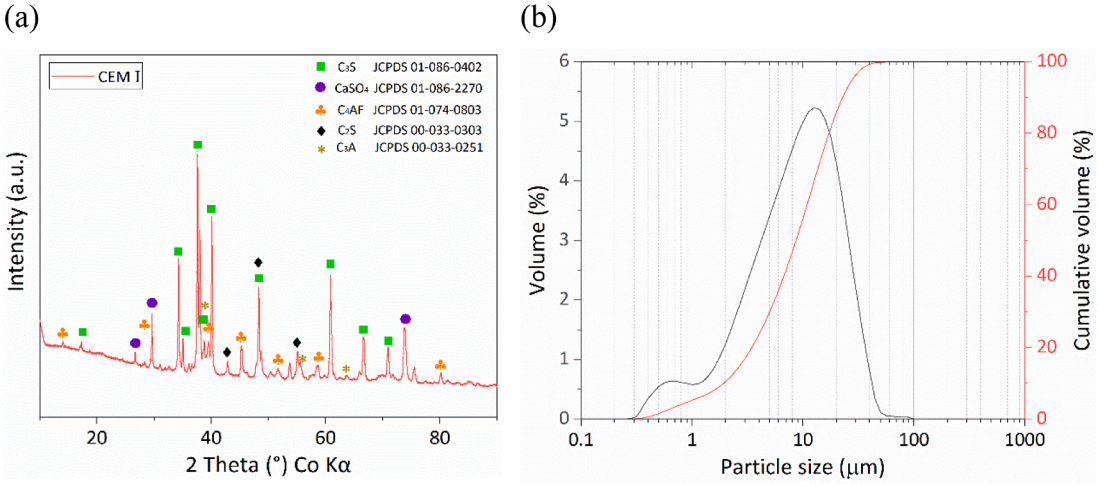

Fig. 1. The phase composition (a) and the particle size distribution (b) of OPC.

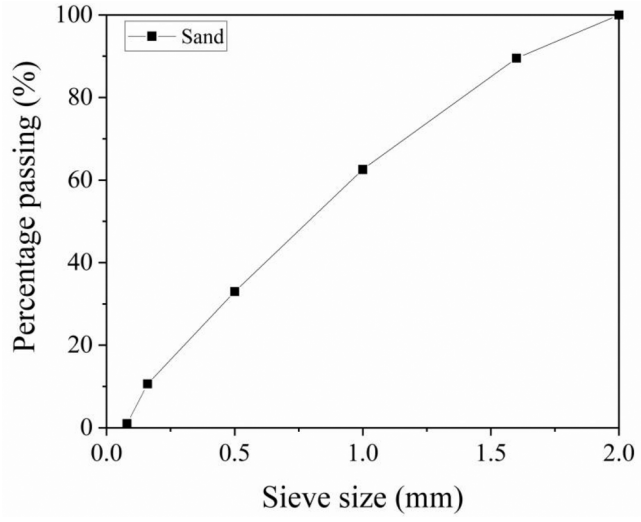

Fig. 2. The particle size distribution of the standard sands used.

Table 4
Sample codes of the different treated fiber-cement composites.

Code	Sand/ Cement	Water/ Cement	Fiber addition (wt% of cement)	Hemp fiber surface treatment
Control	3	0.5	–	–
C-H	3	0.5	1%	Not treated
C-HP	3	0.5	1%	Pretreated only (de-waxing and alkaline treated)
C-HPM	3	0.5	1%	Pretreated and then modified with AKD emulsion

dispersion, which plays an effective role in preventing the growth of the cracks in the composites [39]. In terms of the preparation process, the fibers were first introduced in the cement and sand, and mixed for 90 s in a blender (Perrier Labotest, type 32, France) to obtain a homogenous sample followed by water addition. The matrices, treatments, and weight fractions of fibers are presented in Table 4. After 2 mins, the mixture was cast into a plastic mold (40 mm × 40 mm × 160 mm size) and covered with a damp polyethylene film to avoid water evaporation. One day later, the samples were demolded and cured in a climatic chamber at 20 ± 2 ℃ and 50 ± 5% humidity.

2.3. Characterization

2.3.1. Texture

The surface microphase and structure of modified fibers were analyzed using a Zeiss optical microscope combined with a scanning electron microscope mentioned below. The analyses of the fibers' surface were performed with a Camera/Detector Axiocam 305. Before testing, the fiber samples were made as flat as possible and put on dark paper.

2.3.2. Water absorption test (WAT)

Fiber samples were contained in a steel tea bag and then immersed in distilled water at room temperature. Weight change was recorded by balance every second by a computer program [35], as is shown in Fig. 3. Before measurement, all tested samples were put into the oven (40 ℃, 6 h) to balance the moisture of the fibers.

2.3.3. Fourier transform infrared spectroscopy (FTIR)

The measurements were performed using a Perkin-Elmer spectrometer with wavenumbers ranging from 4000 to 400 cm^{-1}. A total of 4 scans were taken for each fiber sample and corresponding cement composites powder with a resolution of 1 cm^{-1}. To prepare the samples for the FTIR test, AKD-modified fibers were first extracted with acetone to remove the unreacted AKD for 24 h. Then the unmodified and modified fibers were oven-dried at 65 °C for 48 h. More details in some cases are described in ref [40].

2.3.4. Scanning electron microscope coupled with energy dispersive(SEM-EDS)

The surface topography of the fracture surfaces of untreated/treated fibers and fiber-reinforced cement composites was investigated using

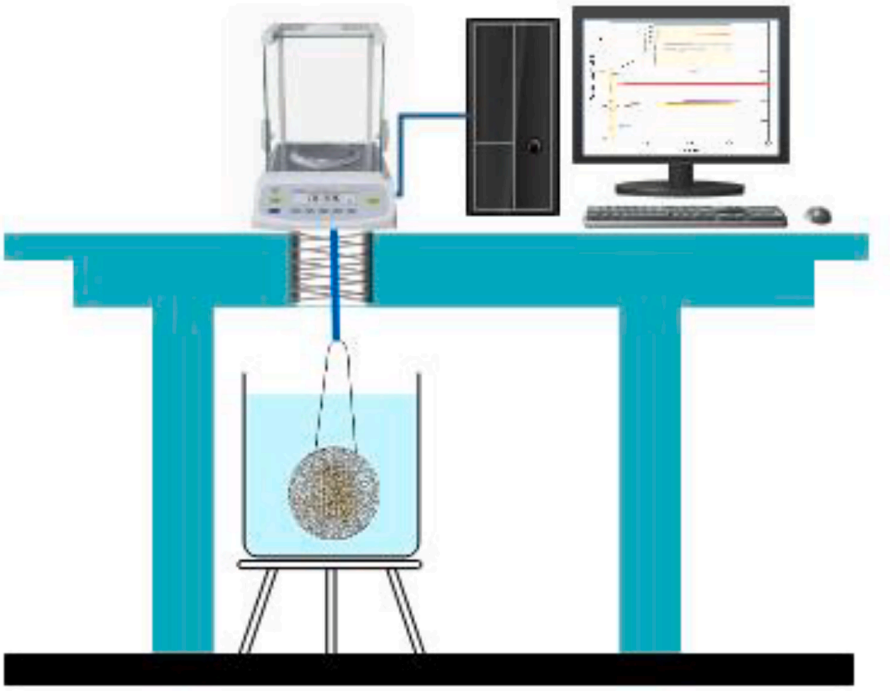

Fig. 3. Schematic diagram of water absorption.

SEM. The micro-surface analyses were performed on specimens covered with Au by using a Thermo Fisher Phenom Pro-X microscope under an accelerating voltage of 15 kV. The chemical composition was identified using energy dispersive spectrometry (EDS) on different spots to verify the presence of hydrated cement on the surface of embedded hemp fibers. For a better representation of the elements present, each sample was chosen to measure in five different embedded fiber regions and an average of the forty values was obtained.

2.3.5. X-ray diffraction (XRD)

The X-ray diffraction (XRD) patterns of fiber-reinforced cement mortars were carried out on ground powder using a Bruker D4 with a Co tube. The angular range was between 10° and 45° (2θ). Before milling into powder for testing, all mortars were cured at ambient temperature after 7 and 28 days. At specific curing ages, the mortar samples were crushed and then immersed in isopropanol. Afterward, the powdered samples were dried in the oven for 24 h at 60 ℃ to stop the hydration process of cement.

2.3.6. Mechanical strength test

The compressive strength and flexural strength were carried out according to EN 196–1 [41]. The three-point bending test was carried out using the EZ 20 Lloyd Instrument (AMETEK) testing machine by AFNOR NF-EN-993–6. All tests were performed using a consistent span of 100 mm and a deflection rate of 0.1 mm per min. At least 5 specimens were tested in a three-point bending configuration for each composite formulation. The value of the load and bending were simultaneously recorded. As we assume that the material is homogeneous, the normal stress σ_{xx} in a rectangular beam of length l between supports is below in Eq. (1):

$$\sigma xx = \frac{3}{2}\frac{Fl}{wh^2} \tag{1}$$

in which F is the applied force, w and h are the width and the height of the beam, respectively.

Significant differences in strength properties between the groups were evaluated using Tukey's HSD test ($P < 0.05$) in JMP Pro 11 software [42]. A new method developed by Barr et al.[43], which is based on ACI Committee Report 544.2R, was adopted to calculate the toughness index (I_t) of the composites in this work. The reason is that the traditional method of calculated toughness index could not be applied with a small percentage of fiber addition which could not provide the typical load–deflection curve. In order to supplementary evaluate the toughness capacity, the post-crack energy absorbed, calculating the area under the load–deflection curve ranging from the post-peak to the end [36]. In addition, the stiffness deriving from the slope of the linear curve

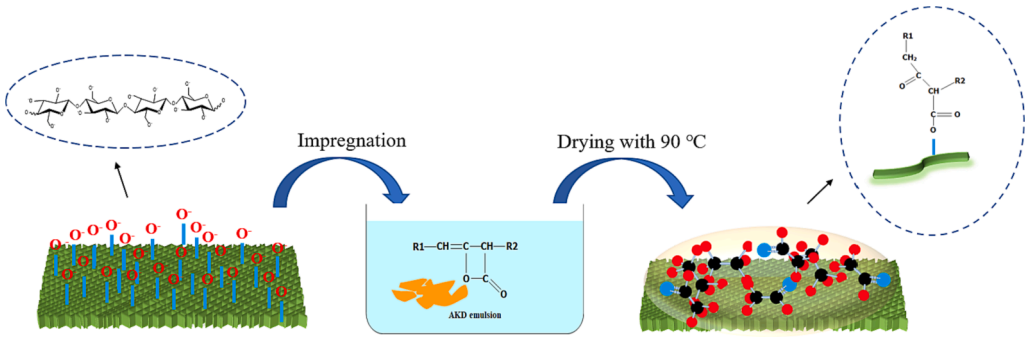

Fig. 4. The schematic illustration of the grafting reaction between pretreated fibers and AKD.

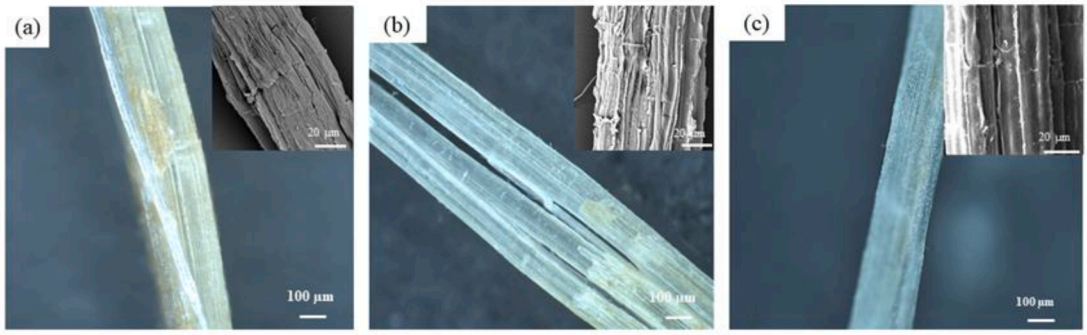

Fig. 5. Micro morphology and structure of fibers with different treatments (a) H, (b) HP, and (c) HPM.

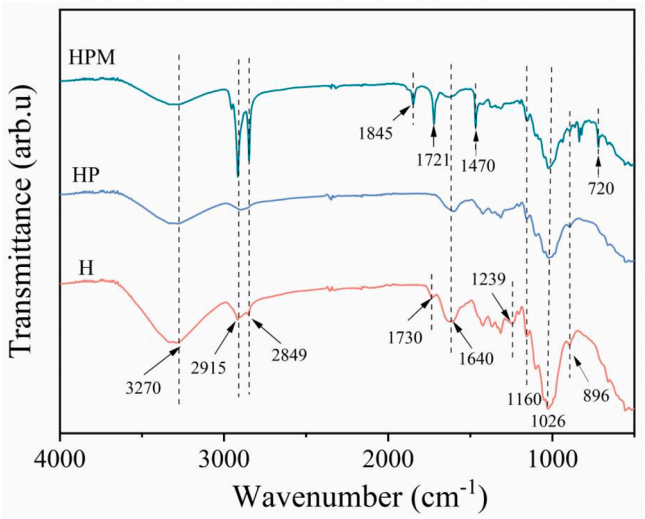

Fig. 6. FTIR curves of H, HP, and HPM.

represents an efficient load transfer process, associated with a good fiber–matrix interface bonding.

3. Results and discussion

3.1. Analysis of fiber modification

3.1.1. The pretreatment and modification mechanism analyses of hemp fibers

Previous studies [28,44] showed that the pretreatment of both sole diluted alkaline solution and a hybrid combination of acetone and alkaline solution could promote the partial removal of lignin, waxes, pectin, hemicellulose, and oils on the surface of natural fiber, and leads to more cellulose OH groups exposed on the fiber surface. It means that the extra hydroxide ions from the alkaline solution readily react with the OH groups on the cellulose chains (mechanism in Eq. (2) which facilitates further chemical modification.

$$\mathrm{Cell-OH + NaOH \rightarrow Cell-O^{-}Na^{+} + H_2O} \quad (2)$$

Therefore, in the second step of modification, the pretreated procedure improves the grafting reaction between the lactone ring of AKD and free OH^{-} groups on cellulosic fibers to form a hydrophobic layer on the fiber surface attributed to a lot of alkyl groups introduced [30,45], as presented in Fig. 4. In this study, the acetone-alkaline pretreatment and AKD modification were performed on hemp fibers. And then the mortar composites reinforced by fibers subjected to different treatments were obtained and analyzed in terms of interface bond and strength performance.

3.1.2. Microstructure of fibers with treatments

The change of the fiber surface morphology is the most direct reflection of treatments. Fig. 5 shows the optical morphology of untreated/treated fibers (Zeiss) and related microstructures under SEM. There are some yellowish substances on the fiber surface presented in Fig. 5(a), which are lignin and waxy substances based on the analyses of FTIR. After pretreatment, this layer of yellow substance almost has been removed, as is presented in Fig. 5(b). Meanwhile, it is observed from the corresponding SEM picture, the surface of the fiber became rougher on account of the removal of partial lignin and other impurities [46].

For the modified fibers, a whitish waxy layer is uniquely coated on the fiber surface which was seen in Fig. 5(c). The micro-level surface of fibers after impregnating is gotten a little smoother but still rather rough. These behaviors are in line with the optical measurements within the CIE Lab system and SEM observation performed by Arminger et al. [47] on the wood surface sprayed with alkyl ketene dimer dispersion.

3.1.3. FTIR characterization of fiber modification

The FTIR analyses reveal the AKD grafting modification on hemp fibers. Fig. 6 shows the infrared spectra of untreated/treated fibers. Plant fibers are primarily composed of three main components: cellulose, lignin, and hemicellulose. In the hemp fibers (H), the peak at around 3270 cm^{-1} represents the stretches of O-H bonds from cellulose and hemicellulose; the O-H bending of absorbed moisture is at 1640 cm^{-1}. The peaks around 1026 cm^{-1} correspond to the C-O of a secondary alcohol, as well as the stretch at 2915 cm^{-1} is the C-H bond from $–CH_2$- of cellulose [48]. In addition, the H spectrum shows that 1160 cm^{-1} and 896 cm-1 represent C-O-C stretching at the β-(1 → 4)-glycosidic linkages in cellulose and hemicellulose [49]. After pretreatment, almost all peaks become weakened and some peaks disappear, which is likely due to the removal of impurities from fibers (e.g. lignin, certain hemicellulose, and wax) [28,44]. For example, the peak at 1239 cm^{-1} of HP is significantly lower than that in the H. The decrease in the peak intensity represents the reduced C-O stretching of the acetyl group of lignin [50,51]. In addition, the peak intensity at 3270 cm^{-1} weakens and even the peak at 1730 cm^{-1}, corresponding to the C = O stretching of the acetyl groups, disappears in the HP [50,52]. These indicate the degradation of lignin and hemicellulose on the hemp fiber surface [50].

In terms of AKD-modified fibers (HPM), this curve, in general, is similar to those of the H and HP but there are still some obvious differences between them. This suggests that the modification treatment of hemp fibers just changes the chemical groups characteristic of the fibers' surface instead of their structure. The stronger intensity of the sharp peaks at around 2915 cm^{-1} and 2849 cm^{-1}, representing symmetric and asymmetric C-H stretching vibrations of $–CH_2$- groups, respectively [53]; the occurrence of new peaks at 1472 cm^{-1} and 720 cm^{-1} is related to C-H scissoring vibration and C-H rock mode [53,54]. These changes indicate that the molecular structure of the HPM surface contains more than four CH_2. This is since the introduction of long-chain AKD molecular provides more alkyl groups and can give good hydrophobicity [53].

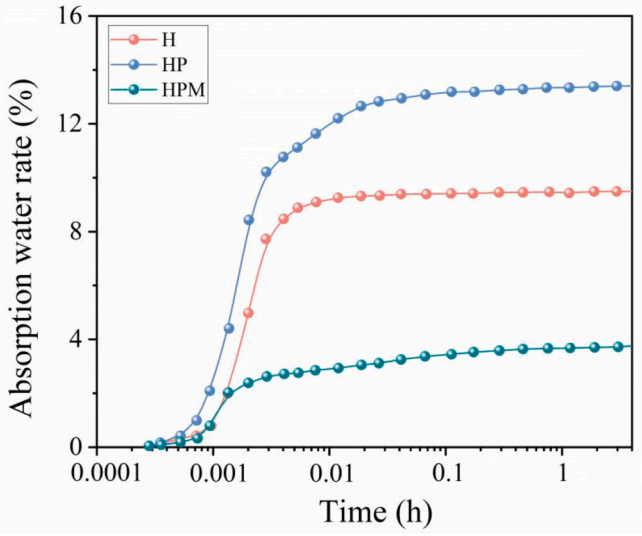

Fig. 7. Absorption water rate curves of fibers with different treatments.

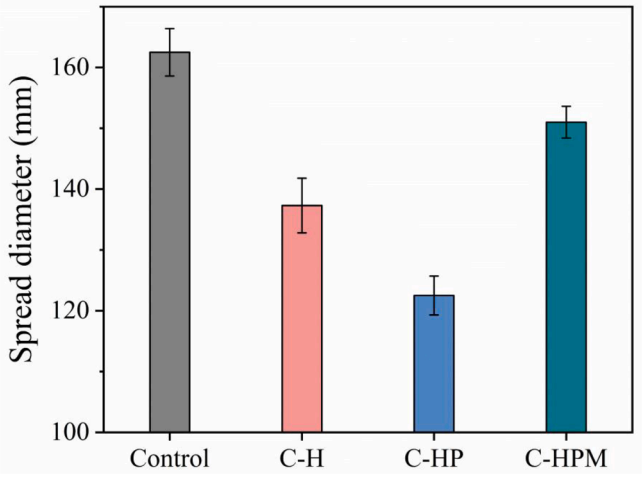

Fig. 8. Variation of spreading of the cement mortar reinforced with or without fibers with different treatments.

Here, it is also worth mentioning that the sharp peaks at 1721 cm^{-1} and 1845 cm^{-1} stand for the C═C double bond and the C═O double bond of the carboxyl group in the AKD lactone ring [45]. Therefore, the above analysis verified that AKD was successfully grafted on the fiber surface.

3.1.4. Water absorption of fibers with treatments

The effect of hydrophobic modification of fibers is justified by water absorption measurement. Fig. 7 shows the water absorption curves for various treated hemp fibers. In general, this result shows that the fibers absorb water very rapidly at first, and later a saturation level was attained without any further increase. In fact, this process of absorbing water, at first, is dependent on both chemical compositions (the hydrophilic groups of the fiber surface) and physical structure (the interweaving gaps among fibers, and fiber voids) and short after mainly on chemistry compositions of fibers (the hydrophilic hydroxyl groups) until the end.

As the treatment varies the water uptake nature of the fibers also varies. It is clear that the HP has the highest water absorption rate while the HPM has the poorest water absorption ability (good hydrophobic effect). This is due to the fact that the pretreated (alkaline pretreated and acetone pretreated) makes the more cellulosic hydroxyl groups exposed on the fiber surface via the removal of lignin and some impurities in the former; however, these hydrophilic groups were replaced with long-chain alkyl groups after the AKD treated in the latter. Therefore, HPM has the best water resistance. This result is consistent with previous finds in the literature [29,45].

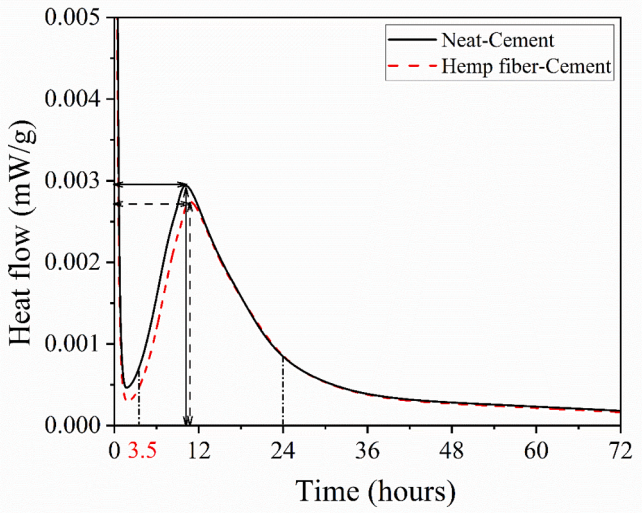

Fig. 9. Heat flow versus time for a typical hemp fiber-cement (dashed curve) and neat-cement (solid curve).

3.2. The analysis of fiber-reinforced cement composites

3.2.1. Workability

The flowability plays an important role in the workability of cement composites, which is reported in Fig. 8. It is clearly shown that fiber-reinforced mortars have relatively poor flowability (120 mm < flow value < 150 mm), compared to the reference mortar without fibers (>160 mm). That could be related to the absorption water of the embedded fibers [55].

Meanwhile, as it can be noted the hydrophobic modification of AKD on fibers somewhat increases the workability of fiber-cement composites (C-HPM > C-H > C-HP) due to the decrease of water demand by the fibers. To some extent, this behavior further confirms the water absorption measurement of fibers (Section 4.1.4).

The fiber-reinforced cement composites are then investigated in terms of compatibility, reaction products, and mechanical strength.

3.2.2. The interfacial compatibility analysis

To directly understand the interfacial bonding of hemp fiber-cement composites, it is crucial to judge the compatibility by a quantitative indicator and qualitative characterization. In this study, the cross-compatibility index (CX) method proposed by Sorin et al. [56] in Eq. (3), was employed to evaluate the compatibility between hemp fiber and cement matrix. Besides, in order to interpret Eq. (3), a typical heat hydration curve is given in Fig. 9.

$$CX = \sqrt[3]{\frac{HR_{max}H_{3.5-24}t'_{max}}{HR'_{max}H'_{3.5-24}t_{max}}} \quad (3)$$

In which HR_{max} = maximum heat rate of hemp fiber-cement composite (mW/g); HR'_{max} = maximum heat rate of neat cement paste

Table 5
The cross-compatibility indexes of hemp fiber-reinforced cement composites.

	Hemp fiber-reinforced cement composites		
	C-H	C-HP	C-HPM
Cross compatibility indexes (CX)	95.9%	97.3%	99.5%

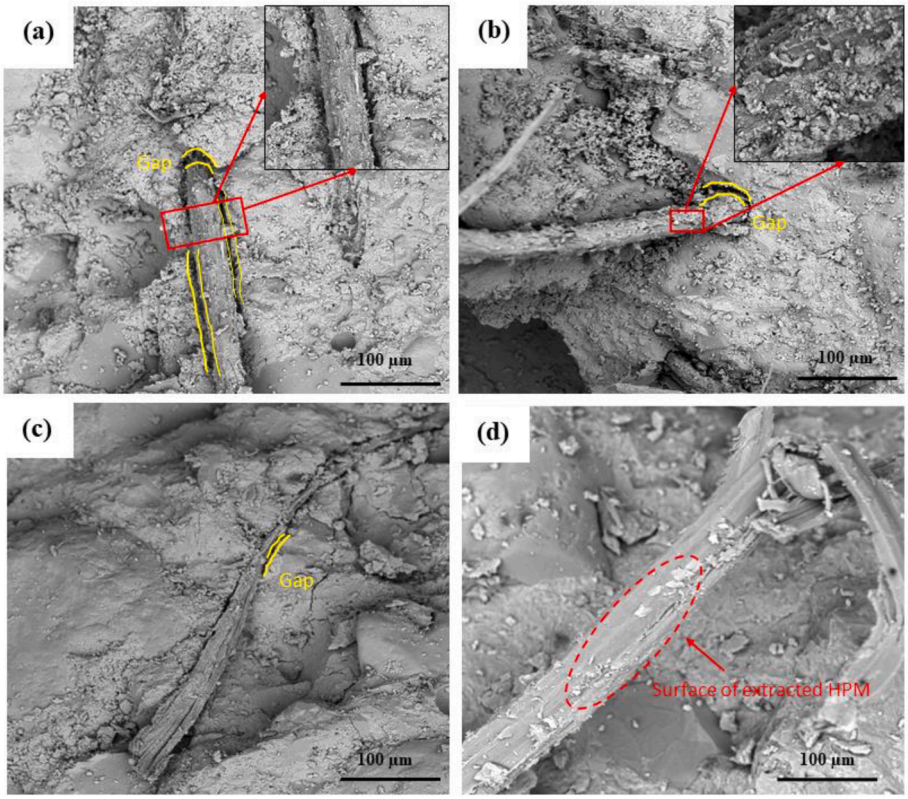

Fig. 10. Interface area of fiber-reinforced cement composites (a) C-H and (b) C-HP, applied zoom indicates the location of cement hydration products, and (c) C-HPM (d) Extracted HPM.

(mW/g); $H_{3.5\text{-}24}$ = total heat (the area under heat rate curve) released by hemp fiber-cement composite in 3.5—24 h interval (J/g); $H'_{3.5\text{-}24}$ = total heat (the area under heat rate curve) released by neat cement paste in 3.5—24 h interval (J/g); t_{max} = time to reach maximum heat rate of hemp fiber-cement composite (h); t'_{max} = time to reach maximum heat rate of hemp fiber-cement composite (h).

Table 5 presents the level of compatibility of the cement composites reinforced with different treated hemp fibers. The hemp fiber-reinforced cement composites exhibit high compatibility index values (above 95.0%), indicating good compatibility between hemp fibers and cement matrix. This could be attributed to the lower content of organic extractives in hemp fibers, resulting in a less inhibitory degree of cement hydration when compared to other plant fibers [57,58]. Among hemp fiber-reinforced cement composites, C-HP and C-HPM have better compatibility levels after 28-day curing. This is associated with the fibers' pretreatment which removes those cement-hardening inhibitory components (some sugars and extractives) which from the hemp fiber surface. Further, C-HPM has the best compatibility level due to the presence of AKD grafted on the fiber surface. This modification layer hinders the capture of Ca^{2+} present in the cement solution by cellulose fibers, benefiting the nucleation of $Ca(OH)_2$ and C-S-H gel and then mitigating the retarding degree of cement hydration [59]. Therefore, the main conclusion is that AKD modification has a positive influence on the compatibility between hemp fiber and cement matrix.

Apart from that, the microstructure and appearance of fiber-cement composites are important for characterizing the interface link situation between the fiber and cement matrix. Results are shown in Fig. 10, different interactions occur between hemp fibers and cement matrics. In all cases, C-HPM (Fig. 10(c)) reveals the tightest gaps between the fiber and the cement matrix indicating the strongest interfacial adhesion. This behavior is in accordance with the compatibility index calculation mentioned above. However, as for the C-H (Fig. 10(a)) and C-HP (Fig. 10 (b)), the gaps between the fibers and the cement matrix are visibly wider. This is due to the shrinking behavior after swelling of embedded H and HP, which leads to debonding of the fiber–matrix interface. Especially for C-HP, the degree caused by the shrinking of fiber cells after moisture loss is very significant on account of the higher water absorption rate after the pretreatment leading to increased swelling. On the other hand, AKD modification can reduce this swelling-shrinking behavior of the fiber by improving the hydrophobic property. Thus, C-HPM has the best interface bonding.

Regarding the surface appearance of the embedded fibers, Fig. 10(d) shows that the HP surface has the largest amount of attached cement hydration products, whereas the surface of HPM has a few hydration products. The amount of hydration products on the H surface is between those of HP and HPM. Therefore, the amount of hydration products on the different fiber surfaces is closely associated with the physiochemical properties of their surfaces. In fact, the cement hydration products deposited on the fiber surface are a process of heterogeneous nucleation and growth. The extent of this process depends on the fiber substrate properties. To be more specific, the low free energy (both the wetting surface and the rough surface) of the fiber substrate facilitates the heterogeneous nucleation and growth of the cement hydration products [60,61]. Among the three fibers, HP with the roughest and most wettable surface has the most hydration products. Compared with H and HP, HPM has the most hydrophobic and relatively smooth surface; thereby, the cement hydration products are rarely deposited on the surface of HPM. The chemical components of hydration products on the fiber surfaces would be discussed below.

3.2.3. *The analysis of the reaction products*

To further clearly clarify the interface reaction products, the surface products of the embedded fibers were analyzed through EDS. Based on the elements of cement hydration products like C-S(A)-H, portlandite (CH), and ettringite, the atomic ratios of several elements with respect to calcium are investigated and shown in Fig. 11.

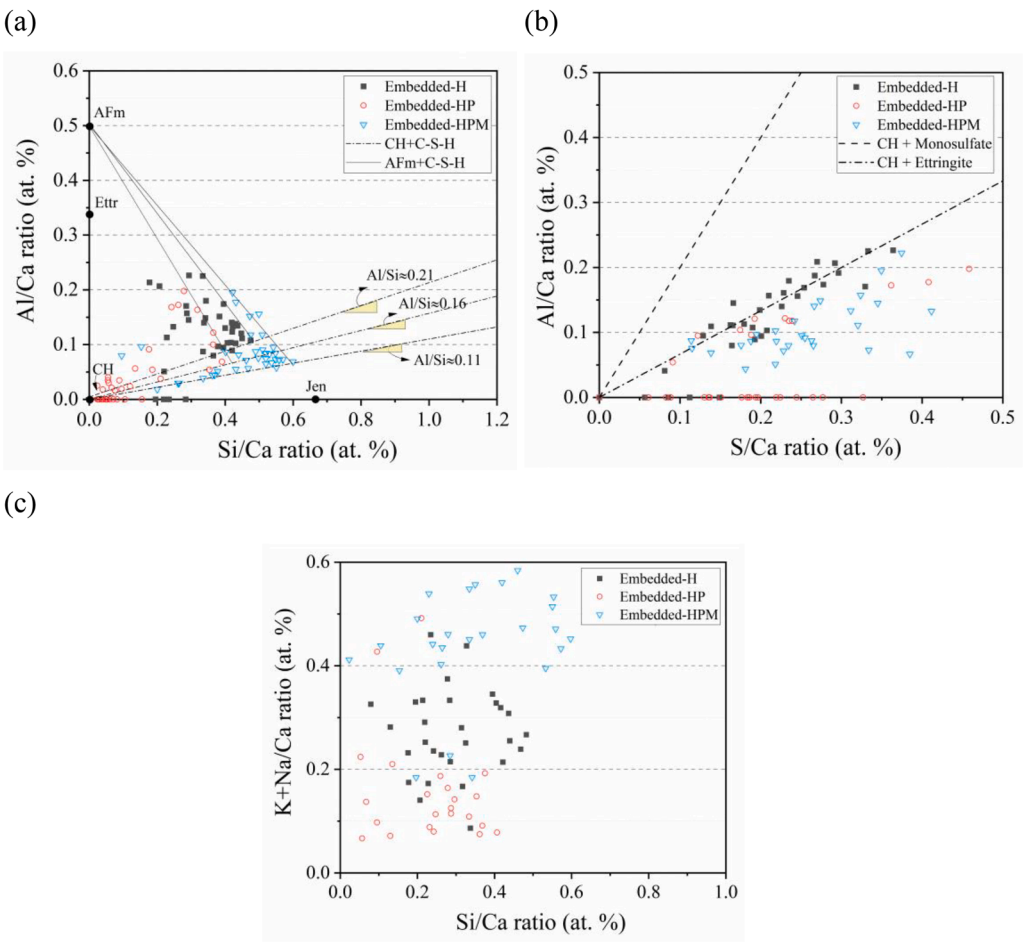

Fig. 11. Al/Ca versus Si/Ca (a), Al/Ca versus S/Ca (b), and K + Na/Ca (c) atomic ratios of hydration products deposited on the surface of the embedded fiber.

As seen in Fig. 11(a), the Al/Si molar ratio (0.11) of the hydration products on the HPM surface is lower than those of H (0.21) and HP (0.16), respectively, indicating that less amount of SiO_4 tetrahedrons was replaced with AlO_4^- tetrahedrons in the amorphous C-S(A)-H deposited on the HPM surface. It was well known that Si-O-Si bonds were stronger than Si-O-Al bonds in terms of the C-S(A)-H [62]. This also assistant confirms the strong interface bond in the C-HPM. Besides, most data points of HP are concentrated near zero point and on the X-axis (Si/Ca), which means more portlandite was precipitated on the surface of HP, which agrees with the literature [63–65]. In Fig. 11(b), the embedded-H data is along the theoretical composition line representing the mix of CH and ettringite, which is average higher than the data distribution of the embedded-HPM. In detail, the range of the S/Ca ratio is similar between both but in terms of the Al/Ca ratio, the data range of the embedded H is higher than that of the embedded HPM. This suggests the composite of CH and ettringite, perhaps more ettringites, on the embedded HPM surface. As regards the alkali content ratio in Fig. 11(c), it can be seen that the data plots of the K + Na/Ca ratio of the embedded-HPM (above approx. 0.40) exceed those of the embedded-H (0.18–0.38) and the embedded-HP (0.06–0.21). This reason for this phenomenon most likely lies in the fact that the hydrophobic characteristic of the HPM surface hinders the alkali ions from entering into the fiber's inner lumen by reducing the swelling capacity, hence more alkali ions stay on the fiber surface. Another potential reason is that the increased formation of the C-S-H phase (as discussed earlier) on the HPM surface enhances the adsorption of alkalis such as K^+ and Na^+, thereby reducing their leaching [66]. The surface of the embedded H has the second-highest K + Na/Ca ratio maybe since the extractives (i.e., pectin and wax) of the H surface ascribed to the untreatment also have a certain hydrophobicity, playing a similar behavior to the HPM. On the hand, the embedded HP facilitates the entry of alkali ions into the fiber structure due to its high water absorption capacity, resulting in less amount of these ions attached to the fiber surface.

To further investigate the impact of different fiber treatments on the hydration products of cement matrices, XRD and FTIR analyses were also carried out in this study. Fig. 12 displays the phase compositions of different samples after 7 and 28 days of curing. In general, all peaks still occur at the same positions irrespective of fiber treatments and the curing time (Fig. 12(a) and (b)). That means, fiber treatments in this study cannot cause the formation of new cement hydration products, which is mainly because the fiber components and chemistry AKD molecular are not involved with the cement hydration reactions. In addition, the intensity of two peaks, representing portlandite and calcite or C-S-H, become obviously stronger due to the cement hydration. It is also interesting to note that no distinct peaks for the embedded fibers were identified. This could be due to the small percentage of fibers compared to cementitious materials.

Another, Fig. 13 depicts the FTIR curves of the fiber-cement composites at different curing stages. In the present experiment, the major vibration bands are identified for cement hydration products. To be more specific, at the 7 days curing stage as is shown in Fig. 13(a-d), the band at 3645 cm^{-1} is due to the OH band from $Ca(OH)_2$ [67]. Whereas the band at around 3405 cm^{-1}, representing hydrogen-bonded OH species, is very wide and weak. To explain this phenomenon, one reason possibly is that the distance forming the hydrogen bonds could be not met as the network of C-S-H gel is relatively loose during 7-day curing. Another possible reason is most OH is presented in the form of free water involved in the early hydration reaction of cement. The band centering

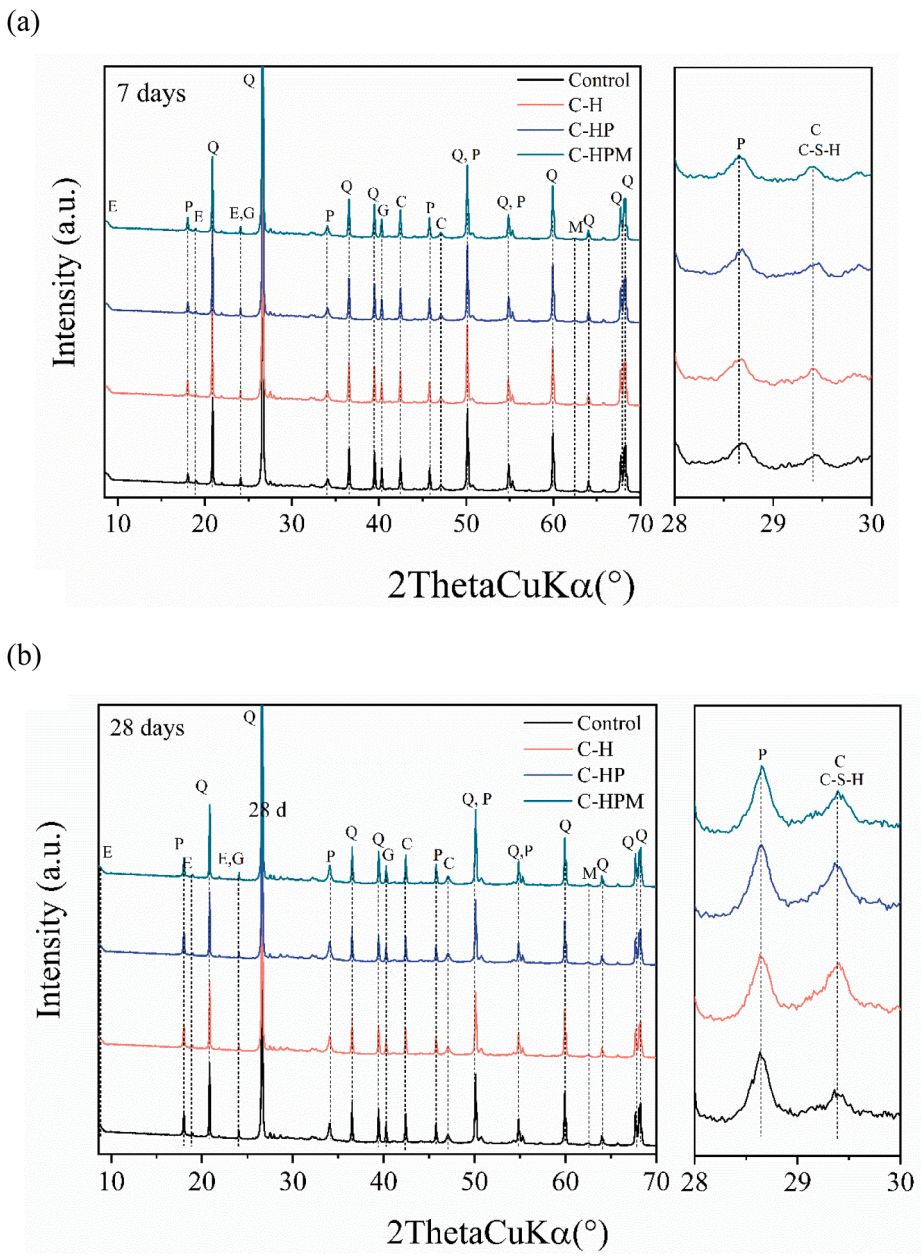

Fig. 12. XRD curves of the cement composites reinforced with or without fibers after curing 7 days (a) & 28 days (b), respectively.

at about 1652 cm^{-1} is caused by the bending vibration (V_2) of irregularly bound water [68,69]. Fig. 13(c) shows the carbonate bands, 1420–1480 cm^{-1}, which arise from the reactions of atmospheric CO_2 with calcium hydroxide [70,71]. The sulfate absorption bands (S-O stretching bands) are assigned at 1097 cm^{-1} and 1151 cm^{-1}, respectively [71]. For the Si-O from the cement, Si-O asymmetric stretching vibration (V_3) of silicate, Si-O out-of-plane bending vibration (V_4) of silicate, and Si-O in-plane bending vibration (V_2) of silicate centered at 925, 522, and 452 cm^{-1}, respectively. These bands assignments are in good agreement with those studies in the literature [72,73]. Moreover, the presence of the bands located at 776 cm^{-1} and 692 cm^{-1} is due to the quartz of sand [74,75].

At the curing stage of 28 days, the band at approximately 3400 cm^{-1} is obviously stronger than that of 7 days of curing in Fig. 13(a'). The hydrogen bonds formed are probably from the interface of the embedded fibers and the cementitious matrix since the interface distance is closer as the cement hydration develops. Also, the shifting characteristics of the absorption peaks in the range 1650–1660 cm^{-1} representing the irregularly bound water (Fig. 13(b')) are influenced by the hydrophobic treatment of fiber with AKD. For other main peaks, the peaks with the carbonate bands become stronger (Fig. 13(c')) while those peaks corresponding to the S-O (sulfate) presented in Fig. 13(d') are relatively weaker in comparison with the curves of 7 days. The reason for this phenomenon most likely lies in the fact that as the cement hydration proceeds, more calcium carbonate is produced and the sulfate is consumed, respectively [76]. Therefore, the main conclusion is that the fiber treatments have a certain impact on the hydration products deposited on their surfaces but little influence on the hydration of the cement matrix.

3.2.4. *Mechanical properties of fiber-reinforced composites*

Strength performance is an important reflection of the compatibility of fiber-reinforced cement composites. The results of the mechanical strength of the samples are displayed in Fig. 14 and summarized in Table 6.

In Fig. 14(a) and (b), almost all fiber-reinforced cement composites

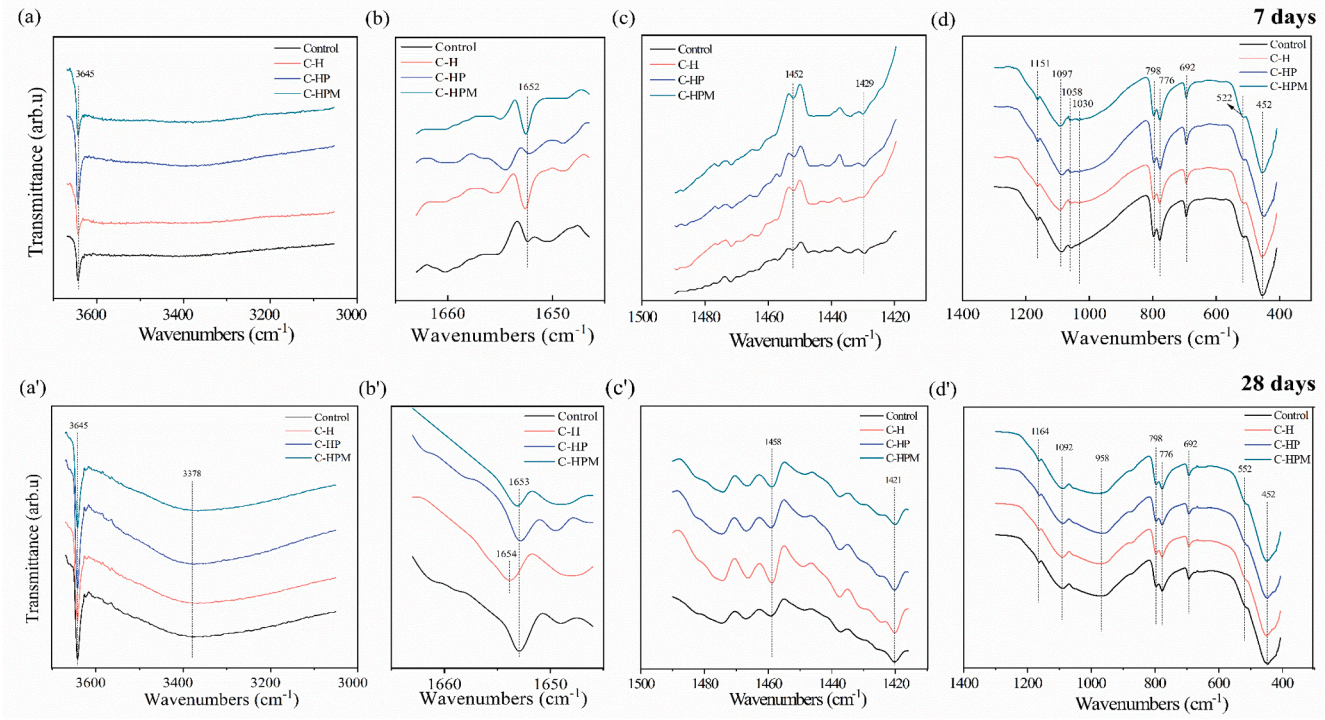

Fig. 13. FTIR curves of the cement composites reinforced with or without fibers after 7 days (a-d) & 28 days (a'-d').

are better than the control at all ages (7 days and 28 days) when hemp fibers at 1.0% by weight of cement weight are mixed into mortars. This may be due to the filling effect of the embedded fibers in the matrix [79]. Similar results have further been reported by other researchers [80,81]: Balasubramanian et al. [80] suggested that the addition of fibers by a dosage of 1.5% could show an increase in compressive strength as compared to conventional concrete. By contrast, the compressive strength of the C-H is slightly lower than that of the control sample at all curing ages. This can be due to the retarding effects caused by hemicellulose-type polysaccharides of hemp fiber, which overtakes its filling effect. Compared to the C-H statistically, C-HP shows significantly higher strength performance. This is related to the pretreatment of embedded fibers which can not only decrease the air-entraining effect [82], which is reflected by the density results but also reduce the delaying effect due to some polysaccharides [83]. Regarding the effect of decreased air entraining, this is due to the fiber pretreatment which leads to the destruction of the surface structure of fibers, thus allowing water to penetrate and displace air that may have been trapped in the voids or lumen structures of the fibers. Finally, this displacement contributes to reducing the overall entrapped air content in the composites. Moreover, it has to mention that the C-HPM in this study has the highest strength properties in all fiber-reinforced cement composites statistically. This could be justified because of the best interface compatibility between the fiber and the matrix (as discussed in sections 4.2.2 and 4.2.3). Interestingly, it can be seen that control samples at 3 and 28 days of curing do not present ideal strength performance. The reason for this phenomenon is unclear but could be attributed to high air humidity that increases the underlying water-cement ratio. This results in a little negative impact on mechanical strength development. In addition, such phenomenon of low expected strength was also found in the previous study [84].

As shown in Fig. 14(c), C-HPM exhibits the highest strength increment, about 33.84% in compressive strength and approximately 28.23% in flexural strength from 7 to 28 days of curing, among all specimens. This can be attributed to the fact that both the AKD modification reduces the swelling-shrinking capacity of fibers and the pretreatment densifies the microstructure of the cement matrix [82,85]. While in the same period, the increment of C-HP is the lowest in compressive strength and flexural strength, which are 10.52% and 10.18%, respectively. In fact, this phenomenon is caused by the characteristic of high water absorption of HP, resulting in the higher swelling-shrinking degree of the embedded fibers and then poor compatibility between the fiber and the cement matrix. The results in Fig. 14(d) indicate that in previous studies the flexural strength improvement of the natural fiber-reinforced cement composites is quite limited even though the addition of fiber content increases. However, the flexural strength in this work (the addition of 1 wt% of cement) is relatively higher due to the swelling-resistant behavior. This increases the potential of hemp fiber-reinforced cement composites applied in the construction field.

The response curves can be evidently described by identifying two domains shown in Fig. 15. The first linear region represents the uncracked stage, and the second region is identified by the development of cement matrix crack (non-linear response is magnified in Fig. 15(b)), fiber pull-out process, and cracked stage, in which crack pattern is completely developed up to failure [36]. The non-linear range is quite limited, which is attributed to the small dosage of fiber in the composites. In general, all cement composites reinforced by hemp fibers show higher peak response and longer displacement compared to the control specimen without fiber addition. Interestingly, C-HP has the highest peak response and longest displacement elongation at 7 days but cured to 28 days is quite low or short in both, just slightly above that of the control in terms of the peak. The reason for this phenomenon most likely lies in the fact that the mechanical interlock is formed between the rough surface of HP and the cement matrix at the early curing time; whereas the high swelling and shrinkage behaviors of HP take responsibility for this as time goes by.

In addition, combined with the results of the toughness index and post-crack energy absorbed in Table 6, the fiber-reinforced cement composites have an increase in both toughness and ductility compared to the plain. Indeed, hemp fibers not only improve the resistance to micro-crack initiation but also bridge the macro-cracks of the cement matrix, thereby delaying the fatigue-crack propagation of composites and increasing the toughness capacity. It is also noted that the C-HPM exhibits the highest stiffness, which is approximately 65% and 12%

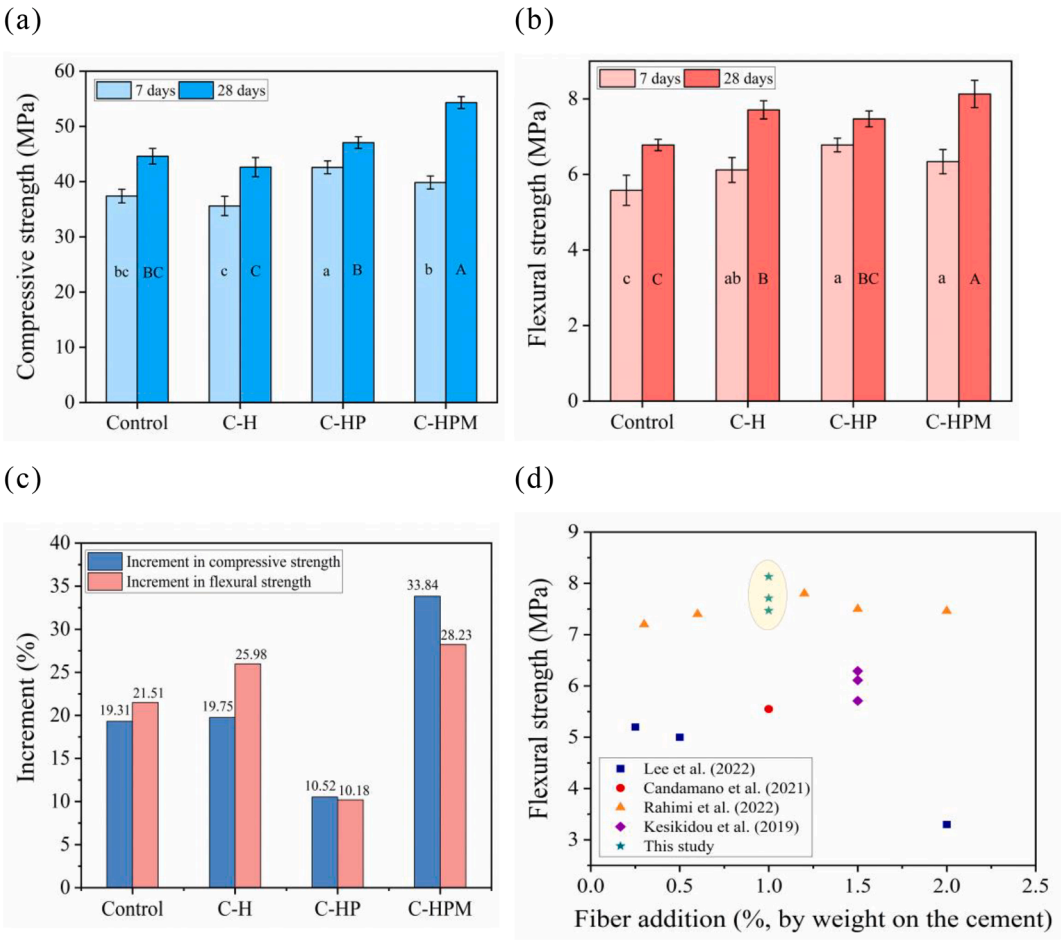

Fig. 14. Compressive strength (a) and Flexural strength (b) of fiber-reinforced cement composites. The composite samples with or part with the same letter in the middle of the columns are not statistically different by Tukey's HSD test; increment percentage in both strength (c) and the comparison of flexural strength data obtained from this study with that of other studies (d) [36,37,77,78].

Table 6
Physical and mechanical properties of the fiber-reinforced cement composites.

		Control	Hemp fiber reinforced composites (1 wt% of binders)		
			C-H	C-HP	C-HPM
Density (Kg/mˆ3)	7 d	2007 ± 3.4	1979 ± 5.3	2053 ± 5.5	2031 ± 10.9
	28 d	2180 ± 7.4	2095 ± 8.1	2177 ± 10.5	2237 ± 6.2
Compressive strength (MPa)	7 d	37.39 ± 1.23	35.60 ± 1.74	42.59 ± 1.16	39.84 ± 1.18
	28 d	44.61 ± 1.41	42.63 ± 1.74	47.07 ± 1.06	53.32 ± 1.08
Increment (%)			19.31%	19.75%	10.52%	33.84%
Flexural strength (MPa)	7 d	5.58 ± 0.40	6.12 ± 0.33	6.78 ± 0.18	6.34 ± 0.32
	28 d	6.78 ± 0.15	7.71 ± 0.24	7.47 ± 0.21	8.13 ± 0.36
Increment (%)			21.51%	25.98%	10.18%	28.23%
Post-crack energy absorbed (10^{-3}J)	7 d	–	96.22	169.89	107.87
	28 d	–	114.41	82.89	140.98
Toughness Index(I_t)	7 d	1	1.06	1.14	1.09
	28 d	1	1.07	1.08	1.16
Stiffness (kN/mm)	7 d	7.59	6.96	9.12	11.46
	28 d	11.17	12.48	11.88	13.95

higher than that of the C-H at 7 days and 28 days, respectively. This indicates that the interface bonding between HPM and the cement matrix promotes efficient transfer under loading (from the cement matrix to the fibers). This analysis is also confirmed by SEM observation and the relevant compatibility calculation mentioned above.

4. Conclusion

In this study, the interface compatibility and mechanical properties of the hemp fiber-cement composites were improved by different treatments of the fiber surface. Optical microscope, SEM, FTIR and WAT were used to characterize the fibers.

In terms of the composites, the CX calculation and SEM were employed to evaluate the interface compatibility; Both the EDS test of the embedded fiber surface and the XRD and FTIR characterization of the composites were used to study the cement reaction products; The mechanical strength, toughness index and stiffness of the composites were also tested. Based on the results obtained in this work, the conclusions are summarized as follows:

(1) The alkali and acetone pretreatments enhance the roughness of the fiber surface but also led to an increase in the water absorption capacity, which could be related to the removal of lignin and some extractives. However, after AKD modification, the fiber became quite hydrophobic thanks to the presence of alkyl groups.
(2) The CX index calculation and SEM observation show that after pretreatment and AKD treatment, the interface compatibility of

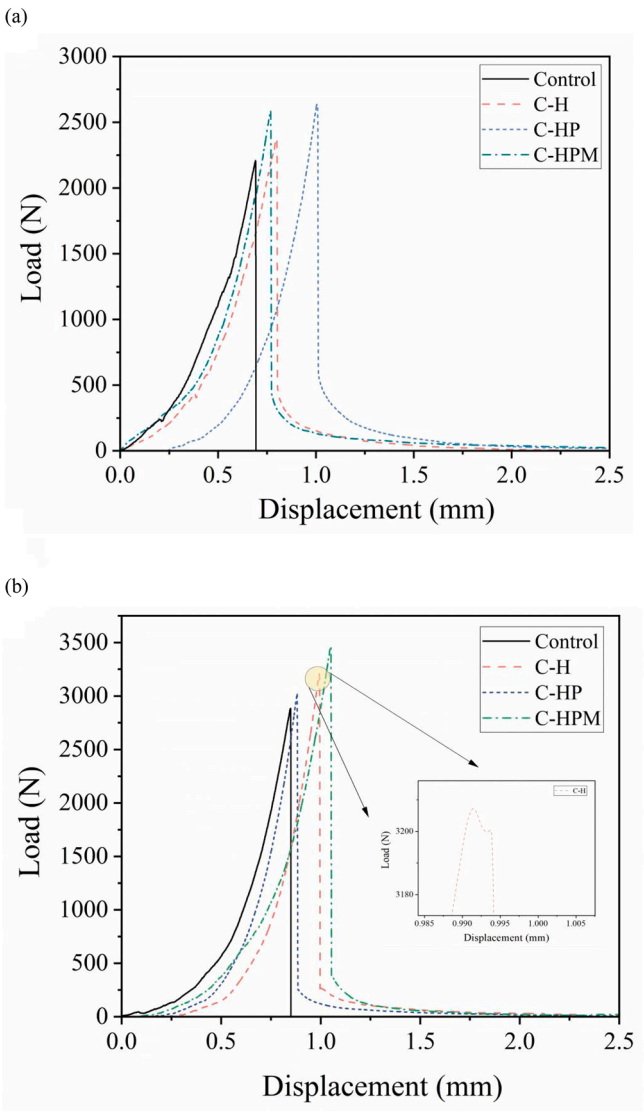

Fig. 15. The load vs. displacement curves of fiber-reinforced cement composites after 7 days (a) and 28 days (b) of curing.

the composites is effectively improved. Therefore, reducing the swelling-shrinking capacity of the fiber is an effective way to strengthen the interface bonding.

(3) Compared with H and HP, less amount of cement hydration products were deposited on the HPM surface. Due to the hydrophobic property (low free energy), the HPM can effectively reduce the heterogeneous nucleation and growth of hydration products on its surface. Furthermore, the portlandite precipitated on the HPM surface accounts for the lower percentage of cement hydration products according to the results of EDS.

(4) There are no significant differences in the hydration products of the cement matrix in the three different composites, indicating that AKD is not involved with cement hydration reaction, a good candidate agent of fiber modification.

(5) The characterization of the mechanical properties showed an increase in the strength performance, toughness capacity, and stiffness for the cement composites reinforced with hemp fibers, especially for the AKD-modified fibers. Thus, this is also a response to the better interface bonding between HPM and the cement matrix.

From these results, it can be concluded that AKD-modified could effectively improve the mechanical properties by strengthening the interface bonding, and be probable in the practical application of the building field.

CRediT authorship contribution statement

Helong Song: Methodology, Data curation, Writing – original draft. **Tao Liu:** Formal analysis. **Florent Gauvin:** Supervision, Writing – review & editing, Visualization. **H.J.H. Brouwers:** Resources, Writing – review & editing.

Declaration of Competing Interest

The authors declare that they have no known competing financial interests or personal relationships that could have appeared to influence the work reported in this paper.

Data availability

Data will be made available on request.

Acknowledgments

This study is supported by the China Scholarship Council (Grant No. 202006150020) and Eindhoven University of Technology. The authors thank Mark Reinders (HempFlax Group, The Netherlands) for the supply of raw fibers, and Marcel Bulten (Kemira, Finland) for the supply of the AKD emulsion.

References

[1] Y. Ma, B. Zhu, M. Tan, Properties of ceramic fiber reinforced cement composites, Cement Concr. Res. 35 (2) (2005) 296–300.
[2] C. Xie, M. Cao, J. Guan, Z. Liu, M. Khan, Improvement of boundary effect model in multi-scale hybrid fibers reinforced cementitious composite and prediction of its structural failure behavior, Compos. B Eng. 224 (2021), 109219.
[3] H. Mitamura, N. Sakata, K. Akashiro, K. Suda, T. Hiraishi, Repair construction of steel deck with highly ductile fiber reinforced cement composites—Construction of Mihara bridge, Bridg. Found 39 (2005) 88–91.
[4] B. Zukowski, E.R.F. dos Santos, Y.G. dos Santos Mendonça, F. de Andrade Silva, R. D. Toledo Filho, The durability of SHCC with alkali-treated curaua fiber exposed to natural weathering, Cem. Concr. Compos. 94 (2018) 116–125.
[5] Q. Wang, Q. Zhu, T. Shao, X. Yu, S. Xu, J. Zhang, Q. Kong, The rheological test and application research of glass fiber cement slurry based on plugging mechanism of dynamic water grouting, Constr. Build. Mater. 189 (2018) 119–130.
[6] R.S. Teixeira, S.F.d. Santos, A.L. Christoforo, J. Payá, H. Savastano Jr, F.R. Lahr, Impact of content and length of curauá fibers on the mechanical behavior of extruded cementitious composites: Analysis of variance, Cem. Concr. Compos. 102 (2019) 134–144.
[7] P. Lertwattanaruk, A. Suntijitto, Properties of natural fiber cement materials containing coconut coir and oil palm fibers for residential building applications, Constr. Build. Mater. 94 (2015) 664–669.
[8] N. Banthia, N. Nandakumar, Crack growth resistance of hybrid fiber reinforced cement composites, Cem. Concr. Compos. 25 (1) (2003) 3–9.
[9] S. Igarashi, A. Bentur, S. Mindess, The effect of processing on the bond and interfaces in steel fiber reinforced cement composites, Cem. Concr. Compos. 18 (5) (1996) 313–322.
[10] H.A. Toutanji, T. El-Korchi, R.N. Katz, Strength and reliability of carbon-fiber-reinforced cement composites, Cem. Concr. Compos. 16 (1) (1994) 15–21.
[11] S. Singh, Polypropylene fiber reinforced concrete: An overview, NBMCW (2011).
[12] P. Soroushian, A. Tlili, A. Khan, Development and characterization of hybrid polyethylene fiber reinforced cement composites, Materials Journal 90 (2) (1993) 182–190.
[13] S. Wang, V.C. Li, Polyvinyl alcohol fiber reinforced engineered cementitious composites: material design and performances. Proc., Int'l Workshop on HPFRCC Structural Applications, Hawaii, Citeseer, 2005.
[14] M.M. Camargo, E. Adefrs Taye, J.A. Roether, D. Tilahun Redda, A.R. Boccaccini, A review on natural fiber-reinforced geopolymer and cement-based composites, Materials 13 (20) (2020) 4603.
[15] J. Wei, C. Meyer, Degradation mechanisms of natural fiber in the matrix of cement composites, Cem. Concr. Res. 73 (2015) 1–16.
[16] J. Wei, Degradation behavior and kinetics of sisal fiber in pore solutions of the sustainable cementitious composite containing metakaolin, Polym. Degrad. Stab. 150 (2018) 1–12.
[17] J. Wei, S. Ma, G.T. D'Shawn, Correlation between hydration of cement and durability of natural fiber-reinforced cement composites, Corros. Sci. 106 (2016) 1–15.

[18] B. Mohr, H. Nanko, K. Kurtis, Durability of kraft pulp fiber–cement composites to wet/dry cycling, Cem. Concr. Compos. 27 (4) (2005) 435–448.
[19] F. Tian, Z. Zhong, Y. Pan, Modeling of natural fiber reinforced composites under hygrothermal aging, Compos. Struct. 200 (2018) 144–152.
[20] R.D. Tolêdo Filho, K. Scrivener, G.L. England, K. Ghavami, Durability of alkali-sensitive sisal and coconut fibers in cement mortar composites, Cem. Concr. Compos. 22 (2) (2000) 127–143.
[21] S. Singh, Alkali resistance of some vegetable fibers and their adhesion with Portland-cement, Research and Industry 30 (2) (1985) 121–126.
[22] N. Janne Pauline S., P. Michael Angelo B., A.C. Kumoro, Hadiyanto, S.A. Roces, L. Yung, X. Rong, A.W. Lothongkum, M.T. Phong, M.A. Hussain, W.R.W. Daud, P.T. S. Nam, Development of abaca fiber-reinforced foamed fly ash geopolymer, MATEC Web of Conferences, EDP Sciences 156 (2018) 05018.
[23] G.H.D. Tonoli, R.F. Mendes, G. Siqueira, J. Bras, M.N. Belgacem, H. Savastano, Isocyanate-treated cellulose pulp and its effect on the alkali resistance and performance of fiber cement composites, Holzforschung 67 (8) (2013) 853–861.
[24] Y. Ban, W. Zhi, M. Fei, W. Liu, D. Yu, T. Fu, R. Qiu, Preparation and performance of cement mortar reinforced by modified bamboo fibers, Polymers 12 (11) (2020) 2650.
[25] K. Bilba, M.-A. Arsene, Silane treatment of bagasse fiber for reinforcement of cementitious composites, Compos. A Appl. Sci. Manuf. 39 (9) (2008) 1488–1495.
[26] E.P. Plueddemann, Nature of adhesion through silane coupling agents, in: E. P. Plueddemann (Ed.), Silane Coupling Agents, Springer US, Boston, MA, 1991, pp. 115–152.
[27] Y. Xie, C.A. Hill, Z. Xiao, H. Militz, C. Mai, Silane coupling agents used for natural fiber/polymer composites: A review, Compos. A Appl. Sci. Manuf. 41 (7) (2010) 806–819.
[28] L. Boulos, M.R. Foruzanmehr, A. Tagnit-Hamou, S. Elkoun, M. Robert, Wetting analysis and surface characterization of flax fibers modified with zirconia by sol-gel method, Surf. Coat. Technol. 313 (2017) 407–416.
[29] G. Garnier, J. Wright, L. Godbout, L. Yu, Wetting mechanism of alkyl ketene dimers on cellulose films, Colloids Surf A Physicochem Eng Asp 145 (1–3) (1998) 153–165.
[30] W. Zhang, X. Yao, S. Khanal, S. Xu, A novel surface treatment for bamboo flour and its effect on the dimensional stability and mechanical properties of high-density polyethylene/bamboo flour composites, Constr. Build. Mater. 186 (2018) 1220–1227.
[31] N. Angin, S. Caylak, M. Ertas, A. Donmez Cavdar, Effect of alkyl ketene dimer on chemical and thermal properties of polylactic acid (PLA) hybrid composites, Sustain. Mater. Technol. 32 (2022) e00386.
[32] K. Missoum, F. Martoïa, M.N. Belgacem, J. Bras, Effect of chemically modified nano fibrillated cellulose addition on the properties of fiber-based materials, Ind. Crop. Prod. 48 (2013) 98–105.
[33] E.M. Salentijn, Q. Zhang, S. Amaducci, M. Yang, L.M. Trindade, New developments in fiber hemp (Cannabis sativa L.) breeding, Ind. Crop. Prod. 68 (2015) 32–41.
[34] A. Mohanty, M. Misra, L.T. Drzal, Surface modifications of natural fibers and performance of the resulting biocomposites: An overview, Compos. Interfaces 8 (5) (2001) 313–343.
[35] N. van Hierden, F. Gauvin, S.S. Lucas, T.A. Salet, H. Brouwers, Replacement of polypropylene fibers by hemp fibers in 3d printed concrete, 4th International Conference on Bio-Based Building Material, 2021.
[36] S. Candamano, F. Crea, L. Coppola, P. De Luca, D. Coffetti, Influence of acrylic latex and pre-treated hemp fibers on cement-based mortar properties, Constr. Build. Mater. 273 (2021) 121720.
[37] M. Rahimi, A. Omran, A. Tagnit-Hamou, Role of homogenization and surface treatment of flax fiber on performance of cement-based composites, Cleaner Materials 3 (2022), 100037.
[38] K. Vandepitte, S. Vasile, S. Vermeire, M. Vanderhoeven, W. Van der Borght, J. Latré, A. De Raeve, V. Troch, Hemp (Cannabis sativa L.) for high-value textile applications: The effective long fiber yield and quality of different hemp varieties, processed using industrial flax equipment, Ind. Crop. Prod. 158 (2020), 112969.
[39] H. Zhang, B. Wang, A. Xie, Y. Qi, Experimental study on dynamic mechanical properties and constitutive model of basalt fiber reinforced concrete, Constr. Build. Mater. 152 (2017) 154–167.
[40] X. Zheng, Z. Liu, T. Fu, S. Easa, W. Liu, R. Qiu, Performance enhancement of asphalt mixtures enabled by bamboo fibers and acrylated epoxidized soybean oil, ACS Sustain. Chem. Eng. 11 (15) (2023) 5867–5875.
[41] E.C.f. Standardization, Methods of Testing Cement-Part 1: Determination of Strength, EN 196-1, 2005.
[42] X. Wu, H. Mou, H. Fan, J. Yin, Y. Liu, J. Liu, Improving the flexibility and durability of aged paper with bacterial cellulose, Mater. Today Commun. 32 (2022), 103827.
[43] K.L. Big Barr, R.C. Dowers, A toughness index to measure the energy absorption of fiber reinforced concrete, The, Int. J. Cem. Compos. Light. Concr. (1982).
[44] F. Sarker, P. Potluri, S. Afroj, V. Koncherry, K.S. Novoselov, N. Karim, Ultrahigh performance of nanoengineered graphene-based natural jute fiber composites, ACS Appl. Mater. Interfaces 11 (23) (2019) 21166–21176.
[45] W. Shen, H. Zhang, R. Ettl, Chemical composition of “AKD vapor” and its implication to AKD vapor sizing, Cellulose 12 (6) (2005) 641–652. %@ 1572–882X.
[46] A. Valadez-Gonzalez, J. Cervantes-Uc, R. Olayo, P. Herrera-Franco, Effect of fiber surface treatment on the fiber–matrix bond strength of natural fiber reinforced composites, Compos. B Eng. 30 (3) (1999) 309–320.
[47] B. Arminger, W. Gindl-Altmutter, J. Keckes, C. Hansmann, Facile preparation of superhydrophobic wood surfaces via spraying of aqueous alkyl ketene dimer dispersions, RSC Adv. 9 (42) (2019) 24357–24367.
[48] F. Veloso de Carvalho, K. Pal, F. Gomes de Souza Junior, R. Dias Toledo Filho, T. Moraes de Almeida, E. Daher Pereira, S. Thode Filho, M. Galal Aboelkheir, V. Corrêa Costa, N. Ricardo Barbosa de Lima, F. da Silveira Maranhão, Polyaniline and magnetite on curaua fibers for molecular interface improvement with a cement matrix, J. Mol. Struct. 1233 (2021) 130101.
[49] J. Zhuang, M. Li, Y. Pu, A.J. Ragauskas, C.G. Yoo, Observation of potential contaminants in processed biomass using Fourier transform infrared spectroscopy, Appl. Sci. 10 (12) (2020) 4345.
[50] W. Liu, A. Mohanty, L. Drzal, P. Askel, M. Misra, Effects of alkali treatment on the structure, morphology and thermal properties of native grass fibers as reinforcements for polymer matrix composites, J. Mater. Sci. 39 (3) (2004) 1051–1054.
[51] N. Sgriccia, M. Hawley, M. Misra, Characterization of natural fiber surfaces and natural fiber composites, Compos. A Appl. Sci. Manuf. 39 (10) (2008) 1632–1637.
[52] J. Biagiotti, D. Puglia, L. Torre, J.M. Kenny, A. Arbelaiz, G. Cantero, C. Marieta, R. Llano-Ponte, I. Mondragon, A systematic investigation on the influence of the chemical treatment of natural fibers on the properties of their polymer matrix composites, Polym. Compos. 25 (5) (2004) 470–479.
[53] P.N. Nelson, Chain length and thermal sensitivity of the infrared spectra of a homologous series of anhydrous silver(I) n-alkanoates, Internat. J. Spectrosc. 2016 (2016) 1–9.
[54] X. Song, F. Chen, F. Liu, Preparation and characterization of alkyl ketene dimer (AKD) modified cellulose composite membrane, Carbohydr. Polym. 88 (2) (2012) 417–421.
[55] S. Beddu, A. Basri, Z.C. Muda, F. Farahlina, D. Mohamad, Z. Itam, N.L.M. Kamal, T. Sabariah, Comparison of thermomechanical properties of cement mortar with kenaf and polypropylene fibers, IOP Conf. Ser.: Mater. Sci. Eng. 1144 (1) (2021) 012036.
[56] S.A. Pasca, I.D. Hartley, M.E. Reid, R.W. Thring, Evaluation of compatibility between beetle-killed lodgepole pine (Pinus Contorta var. Latifolia) wood with portland cement, Materials (Basel) 3 (12) (2010) 5311–5319.
[57] F. Ahmad, H.S. Choi, M.K. Park, A. Review, Natural fiber composites selection in view of mechanical, light weight, and economic properties, Macromol. Mater. Eng. 300 (1) (2015) 10–24.
[58] Z.W. Bin Na, Wood-cement compatibility review, Wood Res. 59 (5) (2014) 813–826.
[59] D. Miller, A. Moslemi, Wood-cement composites: effect of model compounds on hydration characteristics and tensile strength, Wood Fiber Sci. (1991) 472–482.
[60] G. Mascolo, M.C. Mascolo, A. Vitale, O. Marino, Microstructure evolution of lime putty upon aging, J. Cryst. Growth 312 (16–17) (2010) 2363–2368.
[61] A. Myerson, Handbook of industrial crystallization, Butterworth-Heinemann2002.
[62] P. He, M. Wang, S. Fu, D. Jia, S. Yan, J. Yuan, J. Xu, P. Wang, Y. Zhou, Effects of Si/Al ratio on the structure and properties of metakaolin based geopolymer, Ceram. Int. 42 (13) (2016) 14416–14422.
[63] X. Cheng, Y.-B. Li, C.-H. Lu, Effect of pretreatment on the fabrication of natural fibroin fiber/apatite composites using alternate soaking method, J. Inorg. Mater.-Beijing 26 (1) (2011) 43–48.
[64] N. Zhang, H. Ye, D. Pan, Y. Zhang, Effects of alkali-treated kenaf fiber on environmentally friendly geopolymer-kenaf composites: Black liquid as the regenerated activator of the geopolymer, Constr. Build. Mater. 297 (2021), 123787.
[65] A.V. Boehm, S. Meininger, A. Tesch, U. Gbureck, F.A. Müller, The mechanical properties of biocompatible apatite bone cement reinforced with chemically activated carbon fibers, Materials 11 (2) (2018) 192.
[66] B. Mohr, J. Biernacki, K. Kurtis, Supplementary cementitious materials for mitigating degradation of kraft pulp fiber-cement composites, Cem. Concr. Res. 37 (11) (2007) 1531–1543.
[67] M.Y.A. Mollah, Y.N. Tsai, D.L. Cocke, An FTIR investigation of cement-based solidification/stabilization systems doped with cadmium, J. Environ. Sci. Health A 27 (5) (1992) 1213–1227.
[68] M.Y. Mollah, M. Kesmez, D.L. Cocke, An X-ray diffraction (XRD) and Fourier transform infrared spectroscopic (FT-IR) investigation of the long-term effect on the solidification/stabilization (S/S) of arsenic (V) in Portland cement type-V, Sci. Total Environ. 325 (1–3) (2004) 255–262.
[69] T. Richard, L. Mercury, F. Poulet, L. d’Hendecourt, Diffuse reflectance infrared Fourier transform spectroscopy as a tool to characterize water in adsorption/confinement situations, J. Colloid Interface Sci. 304 (1) (2006) 125–136.
[70] K. Suzuki, T. Nishikawa, S. Ito, Formation and carbonation of CSH in water, Cem. Concr. Res. 15 (2) (1985) 213–224.
[71] M.Y.A. Mollah, W. Yu, R. Schennach, D.L. Cocke, A Fourier transform infrared spectroscopic investigation of the early hydration of Portland cement and the influence of sodium lignosulfonate, Cem. Concr. Res. 30 (2) (2000) 267–273.
[72] A. Mollah, D.L. Cocke, M. Yousuf, J.R. Parga, An infrared spectroscopic examination of cement-based solidification/stabilization systems-Portland types V and IP with zinc, J. Environ. Sci. Health, Part A Environ. Sci. Eng. A27 (6) (1992) 1503.
[73] J. Bensted, S.P. Varma, Some applications of infrared and raman spectroscopy in cement chemistry, (1974).
[74] M. Criado, A. Fernández-Jiménez, A. Palomo, Alkali activation of fly ash: Effect of the SiO2/Na2O ratio: Part I: FTIR study, Microporous Mesoporous Mater. 106 (1–3) (2007) 180–191.
[75] W. Tahri, B. Samet, S. Baklouti, F. Pacheco-Torgal, C. Jesus, Mechanical Performance of Geopolymer Mortars Based on Natural Clay, Fly Ash and Metakaolin, European Mortar Summit, 2015.
[76] J. Da, S.A. Neto, A. Torre, A.P. Kirchheim, Effects of sulfates on the hydration of Portland cement -A review, Constr. Build. Mater. 279 (2021), 122428.

[77] G.-W. Lee, Y.-C. Choi, Effect of abaca natural fiber on the setting behavior and autogenous shrinkage of cement composite, J. Build. Eng. 56 (2022) 104719.
[78] F. Kesikidou, M. Stefanidou, Natural fiber-reinforced mortars, J. Build. Eng. 25 (2019), 100786.
[79] Zuo, Junqing, Yao, Wu, Keru, Seebeck Effect and Mechanical Properties of Carbon Nanotube-Carbon Fiber/Cement Nanocomposites, Fullerenes, nanotubes, and carbon nanostructures (2015).
[80] Balasubramanian, J. Chandrashekaran, D. Selvan, Experimental investigation of natural fiber reinforced concrete in construction industry.
[81] K. Korniejenko, E. Frczek, E. Pytlak, M. Adamski, Mechanical properties of geopolymer composites reinforced with natural fibers, Proc. Eng. 151 (2016) 388–393.
[82] Z. Tang, Z. Li, J. Hua, S. Lu, L. Chi, Enhancing the damping properties of cement mortar by pretreating coconut fibers for weakened interfaces, J. Clean. Prod. 379 (2022) 134662.
[83] F. Pacheco-Torgal, S. Jalali, Cementitious building materials reinforced with vegetable fibers: A review, Constr. Build. Mater. 25 (2) (2011) 575–581.
[84] B. Sun, W. Zhao, G. Cai, T. Noguchi, W. Wang, A novel strength prediction model of mortars with different types of cement and SCMs, Struct. Concr. 23 (2) (2022) 1214–1225.
[85] J. Khedari, B. Suttisonk, N. Pratinthong, J. Hirunlabh, New lightweight composite construction materials with low thermal conductivity, Cem. Concr. Compos. 23 (1) (2001) 65–70.